Zoology 114 (2011) 348–359

Contents lists available at SciVerse ScienceDirect

Zoology

journal homepage: www.elsevier.de/zool

Swimming fundamentals: turning performance of leopard sharks (*Triakis semifasciata*) is predicted by body shape and postural reconfiguration

Marianne E. Porter[a,*], Cassandra M. Roque[b], John H. Long Jr.[a]

[a] *Biology Department, Vassar College, 124 Raymond Ave, Poughkeepsie, NY 12604, USA*
[b] *Comparative and Evolutionary Physiology, Department of Ecology and Evolutionary Biology, 321 Steinhaus Hall, University of California, Irvine, 92697-2525, USA*

ARTICLE INFO

Article history:
Received 12 August 2010
Received in revised form 4 April 2011
Accepted 16 June 2011

Keywords:
Body form
Body posture
Body bending
Maneuverability
Yaw turning

ABSTRACT

Turns are essential maneuvers that sharks employ when foraging, feeding, and migrating. How well any individual performs in turning is determined, in part, by the static form and postural reconfiguration of its body. Since the importance of postural reconfiguration in determining turning performance is not well understood, our goal was to examine how body form and posture correlate with turning performance in juvenile leopard sharks, *Triakis semifasciata*. From videos of sharks turning laterally in yaw, performance was measured as turning radius, turning angle, angular speed of the head, and translational speed of the body along its path. Body form variables included the body's length, mass, width, second moment of area, and mass moment of inertia. Postural variables included body-bending coefficient, body flexion at different longitudinal positions, and lag time between body flexion and turning of the center of rotation. Using step-wise linear regression followed by multiple regression, each performance variable was regressed onto three pools of independent variables: (i) all form variables alone, (ii) all postural variables alone, and (iii) a combination of all form and postural variables. From these correlations, it appears that turning performance may be controlled primarily by the magnitude and timing of the flexion of the body. In other words, sharks alter how they turn by changing the pattern in which they bend their bodies; the body acts as a dynamically reconfiguring rudder.

1. Introduction

In animal locomotion, turns are fundamental components of the category of proximal behaviors called maneuvers. Maneuvers, in turn, are characterized mechanically by either translational and/or rotational accelerations of an animal's center of mass (Webb, 2004). In fishes, maneuvers are caused by the forces and torques created by a body whose muscles interact with internal skeletal elements and external fluid, a coupled force system that together changes the body's shape dynamically (Long, 1998; Long et al., 2002a). Changes in the shape of the body, seen as bending in body-caudal fin swimmers (Webb, 1984), are particularly dramatic in turns, when rapid, asymmetric, and transient body bends maneuver fish in escape responses, feeding, foraging, mating, and migration (Webb and Fairchild, 2001; Wu and Wang, 2010). Our goal is to understand how variation in turning performance, measured by the movement of the fish in an external frame of reference, is related to body shape and changes in body shape, measured as form and posture in an anatomical frame of reference.

Body shape has three components (Long et al., 2010): (i) *form*, the static shape of the fish as if it were gliding and holding its body straight; (ii) *posture*, a type of transient shape change imposed on the static form that can be momentary, such as bending the body during a turn, or maintained, such as altering midline curvature or lateral amplitude at different steady swimming speeds (Long, 1995; Long et al., 2002b); and (iii) *undulation*, periodically repeating changes in body shape that create traveling waves of flexure, that are usually but not always propulsive, and that are overlaid on top of form and posture (Root et al., 2007). Each type of shape changes on a different time scale: form changes during development and evolution, posture changes over behavioral time, and undulation changes over propulsive time. This study focuses on how form and posture interact to modulate performance of turns in yaw.

In a yaw turn, the fish rotates about an axis that is perpendicular to the horizontal plane. A yaw turn causes a change in the fish's heading, where change in heading is the most efficient way to describe volitional movement, as demonstrated by stochastic differential modeling of *Kuhlia mugil* (Gautrais et al., 2009). Moreover, the change in heading of fish-like robots is the key control

* Corresponding author. Tel.: +1 845 437 7441; fax: +1 845 437 7315.
E-mail address: meporter@vassar.edu (M.E. Porter).

0944-2006/$ – see front matter © 2011 Elsevier GmbH. All rights reserved.
doi:10.1016/j.zool.2011.06.001

variable for orientation to and navigation up light gradients (Long et al., 2004). The speed of the heading change is used as a measure of agility in fish (Walker, 2000). Explosive changes in heading characterize the yaw-based escape maneuvers in fish and are linked hydromechanically, via momentum flux of the bending body, to locomotor performance (Tytell and Lauder, 2008). Change in heading can be controlled by the bending of the body (Porter et al., 2009), the motion of the caudal fin (Nguyen et al., 2009), or the motion of the head (Wu et al., 2008; Wu and Wang, 2010).

What remains to be understood is if changes in posture, such as the posture characterized during yaw turns by the body-bending coefficient (B_b) which is derived from the simple ratio of the snout-to-tail chord length and the total length of the body, can predict turning performance (Fish et al., 2003). In sharks, form (morphology) of the vertebral column and body predict the magnitude of the change in posture, B_b (Porter et al., 2009). Based on this correlation, we hypothesized that form and posture control turning performance, where turning performance is measured by variables such as turning radius, angular head speed, angular change in the body's center of rotation, and on-path speed of the body. To test this prediction, we examined the routine, volitional yaw turns in freely swimming leopard sharks, *T. semifasciata.*

2. Materials and methods

2.1. Study animals and videotaping

Nine captive leopard sharks, *T. semifasciata* (Triakidae), were filmed on video. They varied in total body length (L_b) from 25.3 to 48.5 cm (Table 1). The distribution of L_b is not normal, with individuals clustering at the ends of the distribution; however, given that we were correlating variation in body shape with variation in swimming performance, we opted to use the entire size range.

Sharks were housed and maintained by staff at the Santa Monica Pier Aquarium, Santa Monica, CA, USA. The Santa Monica Pier Aquarium Director and Head of Animal Husbandry approved these experiments. Filming of sharks took place at the aquarium, and aquarium staff transferred the animals to and from the holding and filming tanks. We were interested in routine turning so we did not elicit startle responses. Animals were filmed immediately after placement into the filming tank.

The filming tank had a footprint of 100 cm × 65 cm and was filled to a depth of 33 cm. The size of the tank and depth of the water were chosen to permit the sharks to swim freely and, at the same time, to encounter walls regularly. Without provocation, sharks routinely swam towards a wall and then turned abruptly. Each individual was filmed for a period lasting no longer than 15 min. Because the sharks swam volitionally, forward translational speed was not controlled and varied within and among individuals.

A video camera (Handycam HDR-HC5; Sony Corp., Tokyo, Japan) mounted 2 m above the tank recorded the free-swimming sharks at 30 frames per second. The continuous recording for each individual was cut into multiple clips, each consisting of one turn in yaw (iMovie HD software, .mov format, 640 × 480 pixels, deinterlaced fields). A yaw turn was defined as a unidirectional, lateral motion of the head greater than 90°, without pushing off the walls or the bottom of the tank (Kajiura et al., 2003).

A total of 118 yaw turns were recorded (Fig. 1). From this sample we chose a single trial for each individual that exhibited their maximum body-bending coefficient (B_b; see Section 2.3 for a definition of this metric). Using LoggerPro version 4.0 (Vernier Software & Technology, Beaverton, OR, USA), seven points on the dorsal midline of the body were manually digitized in each frame of the sequence (Fig. 1). Anatomical landmarks were used for the following points: tip of rostrum (point 1), anterior margin of pectoral fins (point 2), posterior margin of the pectoral fins (point 4),

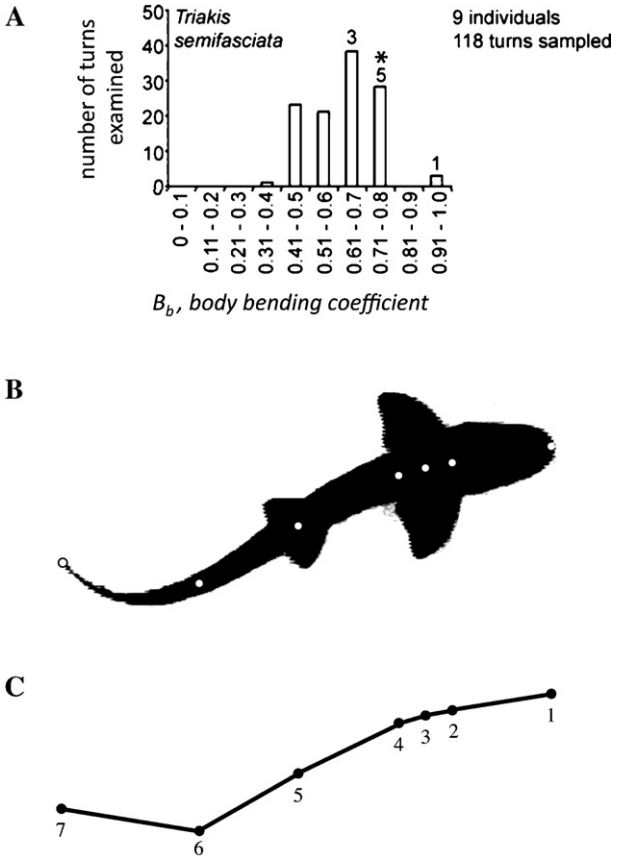

Fig. 1. Screening and analysis of volitional yaw turns in the leopard shark, *Triakis semifasciata*. (A) A total of 118 turns from 9 individuals were videotaped and screened. The turns with each individual's maximal bending coefficient, B_b, were selected for analysis ($n = 9$). The asterisk indicates the mean value of B_b for all trials. (B) Each turn was analyzed by first manually digitizing seven points on the body beginning 1 s before the turn and ending after the turn was complete. Every shark swam steadily, using body-caudal fin undulations, powering into the turn, which was unpowered. (C) The midline of the body, reconstructed in the frame shown in (B) from the digitized points, labeled from head (point 1) to tail (point 7).

middle of pelvic fin insertion (point 5), tip of caudal fin (point 7). In each frame, these five landmarks were digitized first, and then two points were placed midway between two landmarks: middle of the pectoral fins (point 3) and middle of the caudal region (point 6). Digitizing began approximately 1 s before the initiation of the turn (Fig. 2A) to allow preparatory movements, if present, to be analyzed.

Separately, we manually digitized body points (ImageJ software, NIH, USA) to measure the following morphological variables: total length of the body (L_b; in cm), lateral distance between the pectoral fins, a measure of the width of the body (W; in cm). The fineness ratio of the body (F_b) was calculated as the ratio of L_b to W (Porter et al., 2009).

All variable names, symbols, and units are listed in the supplementary electronic Appendix A.

2.2. Kinematic analysis – performance variables

The first class of performance metrics used was based on the translational speed of a body point along its path before, during, and after a turn. For each point on each individual, its translational speed, U (cm s^{-1}), was measured using finite differences in displacement over time. The point with the lowest average U among individuals was used as the proxy for the bodies' center of rotation (CR), since this was the point about which all other points

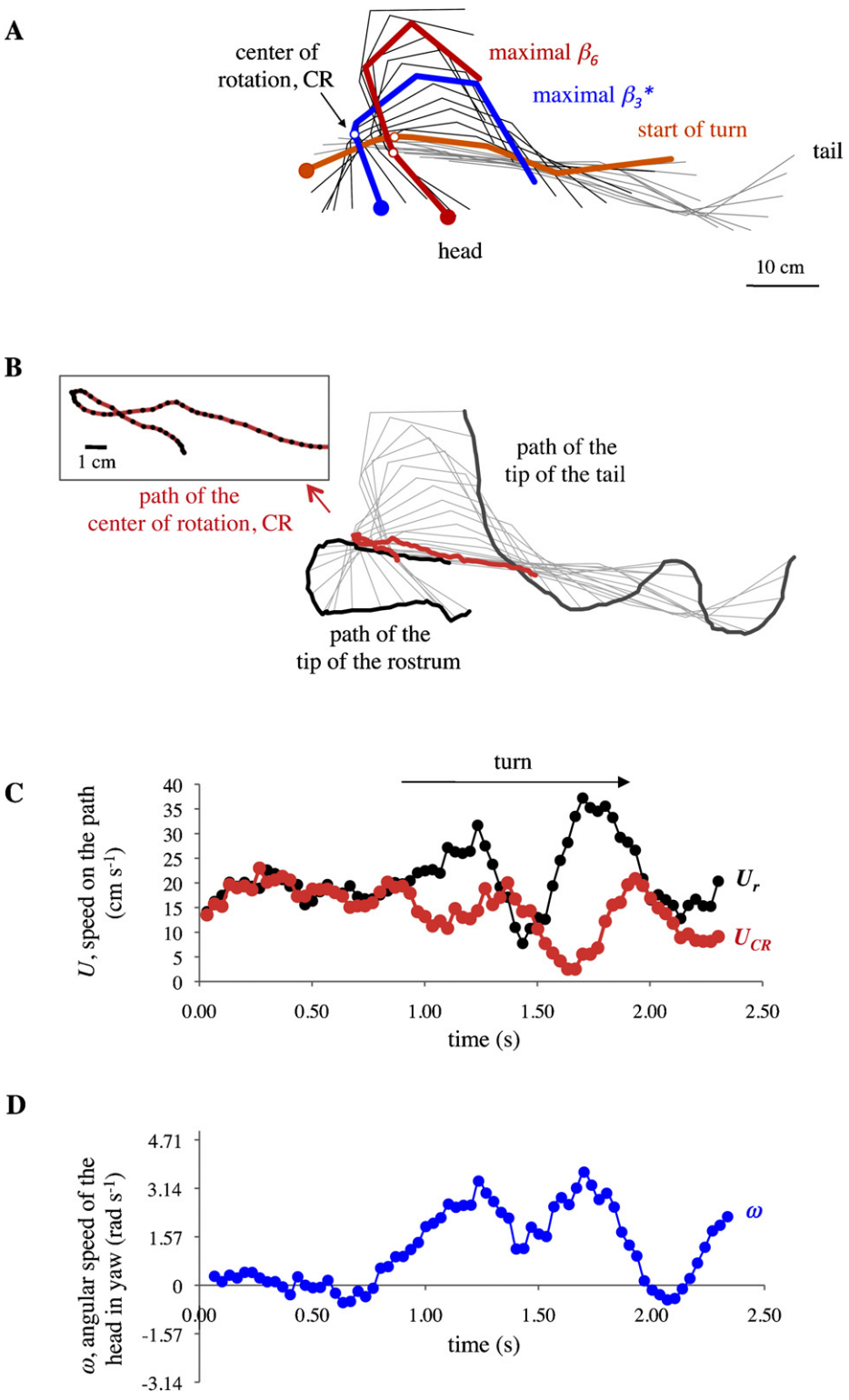

Fig. 2. Turning and turning performance. (A) Turning in yaw. Dorsal view of reconstructed midlines of individual 1 performing a volitional turn in yaw. Gray midlines indicate the motion of the body prior to initiation of the turn. Colored and black midlines indicate the turn. The start of the turn (orange midline) can be defined by a number of variables, including the difference between the speed on the path of the rostrum, U_r, and the center of rotation, CR (see C), the angular speed of the head (see D), and the turning angle of the center of rotation (see Fig. 3A). Time of maximal flexion of the body is indicated by the red midline, when the most posterior joint is maximally flexed as measured by β_6, and by the blue midline, the time when the joint at the CR, point 3, is maximally flexed as measured by β_3^*. The CR, point 3, is indicated on the colored midlines by the hollow circle. (B) The path of points on the midlines can be reconstructed and analyzed to quantify turning performance. The CR (pink line) is, by definition, the point on the body that undergoes the least average displacement among all individuals during the turn. Inset: Note that the CR moves to the left and then reverses direction with a very small turning radius. The path of the tip of the rostrum (black line) also reverses direction, but with greater displacement and larger turning radius. The gray midlines between the CR and the tip of the rostrum indicate the yaw of the head. The path of the tip of the tail (gray line) does not reverse course in this analysis window, indicating, as shown by the midlines, that the shark has not resumed swimming. (C) Speed of the CR, U_{cr} (pink points), and the tip of the rostrum, U_r (black points), along their respective paths. During the turn, the speed of the two points deviates, with the rostrum traveling faster than the CR at almost all times. (D) The angular speed of the head in yaw, ω, is calculated as the rate of change in the angular position of the head. Note that most of the changes in the patterns of path and angular speed occur in a window of approximately 1 s, from about 1 to 2 s. The example data shown here are from the turn of individual 3.

Table 1
Body form of juvenile leopard sharks, *Triakis semifasciata*.

Shark	L_b (cm)	W (cm)	F_b	m_b (kg)	I_a (m^4)	CR	PD	k'_E (m^2)	k'_b (m)	I_m (kg m^2)
1	47.35	4.53	10.45	0.39	2.1E−07	3	0.235	9.2E−07	2.0E−06	0.0024
2	48.53	5.03	9.66	0.42	3.1E−07	2	0.26	1.3E−06	2.7E−06	0.0034
3	25.3	2.13	11.89	0.06	1.0E−08	3	0.28	1.5E−07	6.2E−07	0.0001
4	25.72	2.31	11.16	0.06	1.4E−08	3	0.27	2.1E−07	8.2E−07	0.0001
5	45.69	4.50	10.16	0.35	2.0E−07	4	0.24	9.6E−07	2.1E−06	0.0021
6	28.76	2.36	12.18	0.09	1.5E−08	2	0.27	1.9E−07	6.4E−07	0.0003
7	30.31	2.88	10.51	0.10	3.4E−08	4	0.26	3.7E−07	1.2E−06	0.0003
8	33.94	3.20	10.59	0.14	5.2E−08	4	0.27	4.5E−07	1.3E−06	0.0006
9	27.54	2.71	10.17	0.08	2.6E−08	3	0.265	3.5E−07	1.3E−06	0.0002

L_b, total length; W, body width; F_b, fineness ratio; m_b, mass; I_a, second moment of area; CR, center of rotation position; PD, Proportional distance of CR from rostrum; k'_E, stiffness index of Euler buckling; k'_b, stiffness index of bending; I_m, mass moment of inertia.

appeared to rotate during the turn (Fig. 2B). Because the mode, median, and mean of CR were point 3, this was the point used. Variation in the position of the CR among individuals (Table 1) means that the use of a fixed CR at point 3 across individuals will overestimate speed of the CR in some cases. In sum, for each individual, the maximal U of the CR (U_{cr}) and the rostrum (U_r) were used as two indicators of each individual's performance in turning (Fig. 2C).

A second class of performance metrics used was based on the angular speed (rad s^{-1}) of the head in yaw, ω (Fig. 2D). The first of three yaw-based metrics was the maximal angular speed of the head (ω_{max}) occurring at any point during the turn. It was measured as the largest finite difference of the head's yaw rotation, α, per unit time, the interframe increment of 0.033 s. The head's α was measured as the yaw (lateral) rotation of the line between points 1 and 2 (see Fig. 1) from frame to frame. Two measures of average ω were also taken. The initial angular speed of the head (ω_a) was measured as the ratio of the first 90° of the head's yaw rotation, α, and the time it took the head to traverse that angular distance. Ninety degrees was chosen as the angular distance over which angular speed was averaged because of the convention that a "sharp turn" is one of 90° or more (Kajiura et al., 2003). The secondary angular speed of the head (ω_b) was measured as the ratio of yaw rotation, α, from 90° to the end of the turn and the time it took the head to traverse that angular distance.

A third class of performance metrics, turning angle, ϕ (rad), of the CR, was measured. Using the law of cosines, turning angle of the CR was measured at each time step as the angular deviation of the CR from a straight path, where the straight path was extrapolated from the line drawn between the position of the CR at the previous two time steps. First, to characterize the performance of each individual, the maximal turning angle (ϕ_{max}) was used (Fig. 3A). Second, to account for the possible influence of unequal path steps on the geometry, ϕ_{max} was normalized by the distance of the path steps, ϕ^*_{max} (rad cm^{-1}). Third, using each instantaneous ϕ and its two adjoining path distances, we calculated the instantaneous turning radius (R, in cm) of the CR (Fig. 3B). The minimum turning radius (R_{min}) was used to measure performance.

2.3. Kinematic analysis – independent variables

Body form and posture variables (see Section 2.2. and Appendix A) were used as independent variables to predict turning performance. In addition to the form variables already mentioned, L_b, W, and F_b, we also estimated the mass of the body (m_b) from growth curves (Smith, 1984). We estimated the body's maximal second moment of area, I_a (m^4), and the body's mass moment of inertia, I_m (kg m^2), as follows:

$$I_a = \frac{\pi(W/2)^4}{4}$$

and

$$I_m = \frac{m_b L_b^2}{32}.$$

As a first approximation, we assumed that half of the m_b acts at two points, each located one-quarter of the distance from the tips of the head and tail, each rotating about the mid-point of the body. To assess the possible contributions of body form to the structural stiffness of the body, k (N m^{-1}), we assumed that the apparent Young's modulus of the body, E (Pa), was constant. This assumption of constant E allowed two stiffness indices to be developed. The first index was based on the formula for k (Long et al., 2010) from cantilevered bending of the body, k'_b (m), and the second was based on the formula for the critical load that causes a column to undergo Euler buckling, k'_E (m^2):

$$k'_b = \frac{I_a}{L_b^3}$$

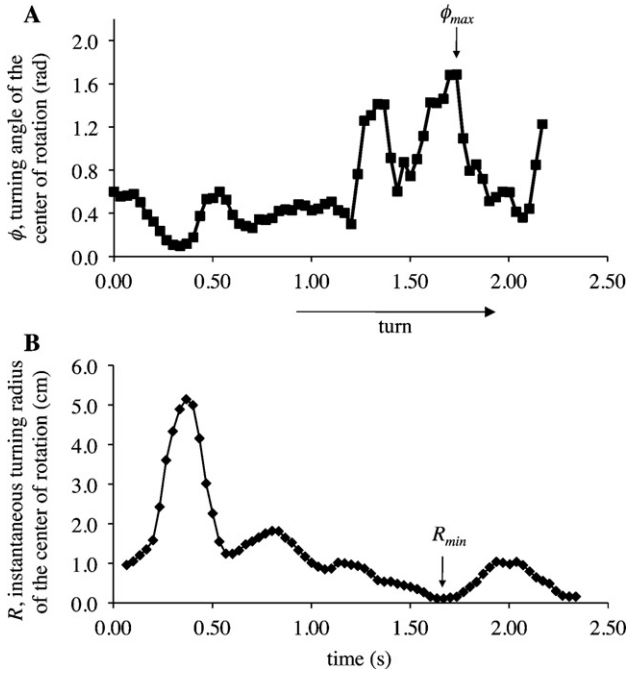

Fig. 3. Turning angle and turning radius of the body's center of rotation, CR. (A) The turning angle, ϕ, of the body's CR is calculated as the deviation of the CR's path from a straight line from one time point to the next. The maximal value, ϕ_{max}, during the turn is used to measure performance. (B) The instantaneous turning radius, R, of the body's CR is calculated as the distance of the CR from the origin of a circle whose perimeter intercepts the tangent of the CR's path. R is inversely proportional to the instantaneous curvature of the path, and the minimal value, R_{min}, is used to measure performance. The sample data shown here are from the same turn as shown in Fig. 2. Signals are low-pass filtered with a five-point running average.

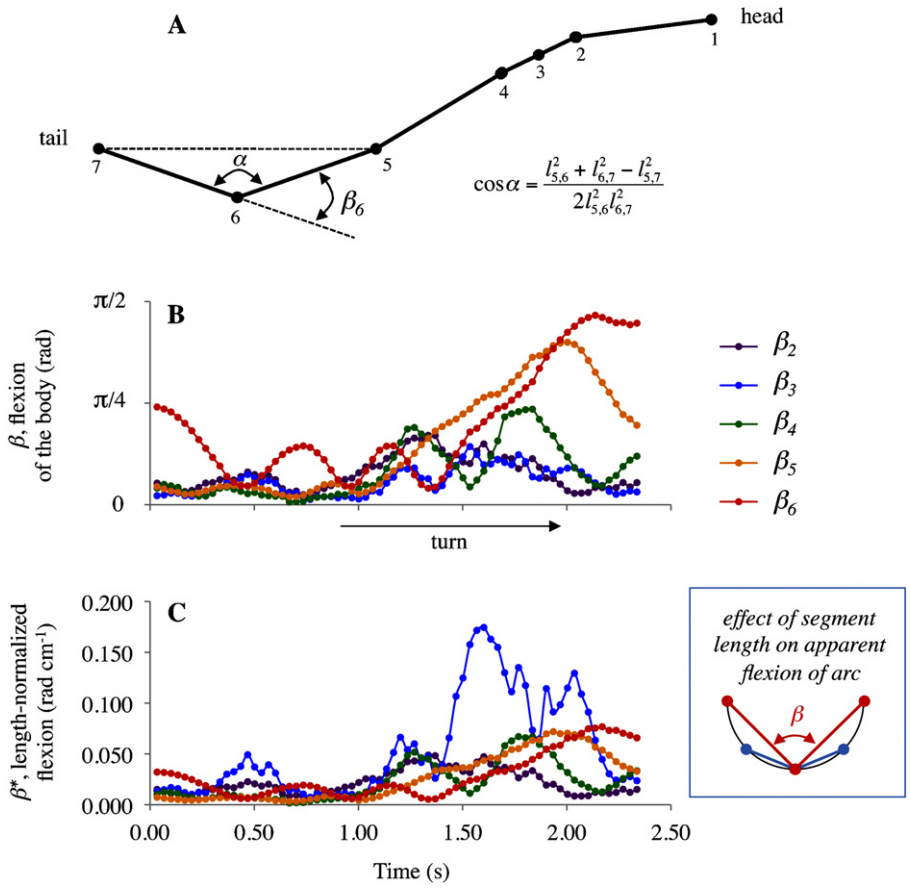

Fig. 4. Postural reconfiguration during a volitional turn. Calculating flexion, *b*, of the body's midline. (A) The law of cosines was used to convert line segments (l) into angles (α) at each of the interior midline points, 2 through 6. Flexion of the body (β) was calculated as the difference between π and α. Left- and right-side flexions are not distinguished. (B) Flexion values over time in a turning leopard shark, from the powered approach to the turn, 0 to about 1 s, to the turn itself (horizontal arrow). Clear increases in β, staggered in time, can be seen at positions 4, 5, and 6. (C) Length-normalized flexion, β^*, also shows the large relative magnitude of the flexion at point 3, near the center of the body's rotation. Inset: The lengths used for normalizing β are the segment lengths; longer segments lengths (red lines) overestimate the β of a circular arc (black line) compared to segments of shorter length (blue). Dividing β by length provides an adjustment for this effect. The sample data shown here are from the same turn as shown in Fig. 2.

and

$$k'_E = \frac{I_a}{L_b^2}.$$

Postural reconfiguration was measured in a number of ways. First, curvature of the whole body was estimated by the body-bending coefficient (B_b), a dimensionless number calculated as the difference between 1 and the ratio of L_c and L_b, where L_c is the chord length between the tip of the rostrum and the tip of the tail (Azizi and Landberg, 2002; Kajiura et al., 2003). While B_b can be calculated at any time before or during a turn, we used only the maximal value for each individual. Second, postural reconfiguration was measured as flexion of the body, β (rad), the angular deviation from a straight line for the body's midline at points 2, 3, 4, 5, and 6 (Fig. 4A). The maximal values at each point during a turn were β_2, β_3, β_4, β_5, and β_6 (Fig. 4B and C). To account for the effects of the different lengths of the segments used to calculate flexion, length-normalized flexions, β_2^*, β_3^*, β_4^*, β_5^*, and β_6^*, were also calculated (Fig. 4D). The sum of the five maximal flexions and five length-normalized flexions, $\sum\beta$ and $\sum\beta^*$, respectively, were also used to characterize posture.

Finally, we measured how postural reconfiguration and locomotor performance were coordinated through time during a turn. Coordination was measured by examining – for the five non-terminal midline points, 2 through 6 – the lag time, δ (s), between ϕ and β_i, where the subscript i indexes all five of the points in turn. The δ_i for each point was calculated as a single number, the time from the start of the turn, which is determined by ϕ, to the time at which β_i is maximally correlated with ϕ (Fig. 5).

2.4. Statistical analysis

All statistical tests were performed with JMP software version 5.0.1.a (SAS Institute Inc., Cary, NC, USA). Using one-way ANOVA with body position as the independent variable, β, β^*, and δ were all tested to see if they differed by body position (significance level = 0.05). One-way ANOVA was also used to test for differences between related variables, U_r and U_{cr}, and the three kinds of ω.

To determine how body form and postural reconfiguration correlate independently and in combination with each performance variable, three different tests were run. For example, the performance variable U_{cr} was used as the response in a step-wise linear regression (mixed direction, $p = 0.25$ in and out) that included as candidate predictors all of the body form variables (see Appendix A). The selected candidate variables were then used in a multiple linear regression of U_{cr} onto the candidate pool. This process was repeated for the postural reconfiguration variables alone and for the form and postural variables combined. Thus, each performance variable was examined using three statistical models: body form, postural reconfiguration, and the composite model, which includes both body form and postural reconfiguration variables. Before

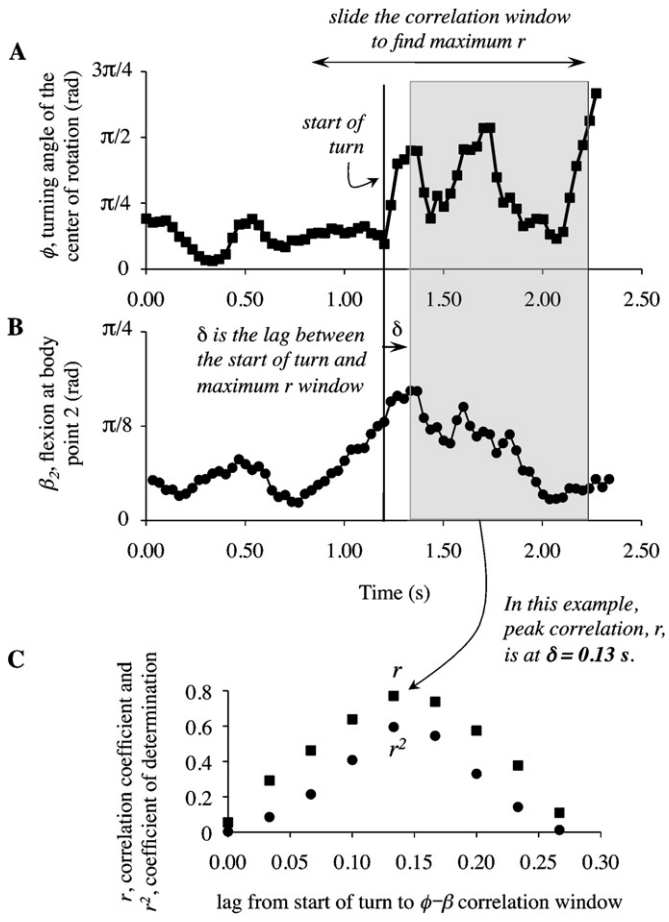

Fig. 5. Lag time, δ, between the start of the turn and the peak correlation between the body's turning angle, ϕ, and the body's flexion, β. By comparing the δ values for non-terminal points on the body, we can assess how the body acts as a dynamic rudder to create and control the turning maneuver. For example, a positive δ value, like the one shown in this example for body point 2, means that β correlates with ϕ after the turn has been initiated. All flexion points are analyzed in a similar fashion.

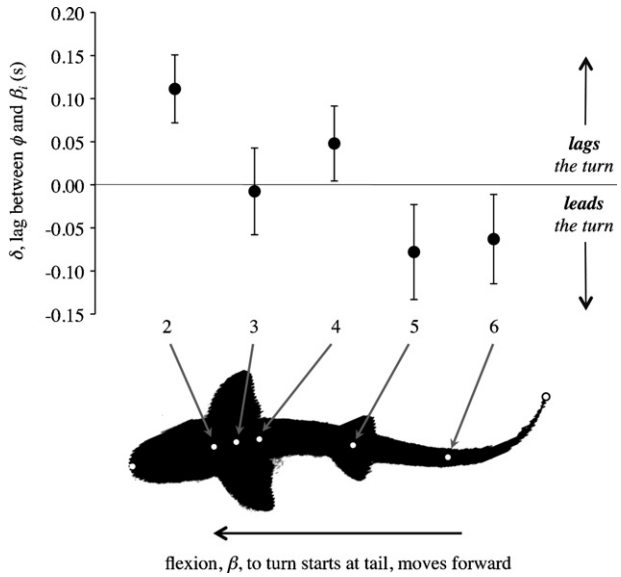

Fig. 6. Dynamic rudder model of a turning shark. Before the turn starts, the turning angle of the CR is maximally correlated with the flexion of the caudal region of the body. After the turn starts, the turning angle of the CR is maximally correlated with the flexion of the precaudal region of the body (points 2 through 4). These differences in timing suggest that the caudal region (points 5 and 6) initiates the turn and that the precaudal region carries it out. Thus the body is a dynamic rudder, operating over time to control these maximal volitional turns. Means ± standard error ($n = 9$). Lag, δ, decreases along the length of the body ($F_{4,40} = 4.99$; $p = 0.0023$).

candidate variables are selected, each model can be represented by the following general notations:

$$\text{form}: \quad y = f(F_b, I_a, I_m, k_b', k_E', L_b, m_b, W),$$

$$\text{posture}: \quad y = f(B_b, L_c, \beta_2 \ldots \beta_6, \Sigma\beta, \beta_2^* \ldots \beta_6^*, \Sigma\beta_i^*, \delta_2 \ldots \delta_6),$$

$$\text{composite}: \quad y = f(F_b, I_a, I_m, k_b', k_E', L_b, m_b, W, B_b, L_c, \beta_2 \ldots \beta_6, \Sigma\beta, \beta_2^* \ldots \beta_6^*, \Sigma\beta_i^*, \delta_2 \ldots \delta_6),$$

where y denotes any of the eight response variables that measure turning performance, and $f()$ denotes "some function of" the independent variables in the accompanying set.

3. Results

L_b of *T. semifasciata* in this study ranged from 25.3 to 48.35 cm, and m_b of the largest animal was 7 times greater than that of the smallest (Table 1). The position of the CR had a mean of 3.1 (SD 0.78), a median of 3, and a mode of 3 (range 2–4). The proportional position of the CR had a mean of 0.261 of L_b (SD 0.0147) (Table 1).

L_b was significantly greater than W, and these body proportions are reflected in the two-dimensional body shape as measured by the fineness ratio, F_b. The lag, δ, between flexion of the body and angular motion at the CR decreased significantly along the length of the body ($F_{4,40} = 4.994$, $p = 0.0023$; Fig. 6). Maximal flexion, β, increased significantly along the length of the body ($F_{4,40} = 29.95$, $p < 0.0001$; Fig. 7), and β_6 was more than double the magnitude of β_2. Length-normalized body flexion, β^*, also varied significantly depending on the point along the body ($F_{4,40} = 7.88$, $p < 0.0001$; Fig. 7). Length-normalized flexion was greatest at point β_3^* and decreased towards the tail. The speed of the rostrum, U_r, was significantly faster than the speed at the CR, U_{cr} ($F_{1,16} = 21.14$, $p = 0.0003$; Table 2). Angular speeds of the head, ω_a and ω_b, were indistinguishable, but were significantly lower than ω_{max} ($F_{2,24} = 8.326$; $p < 0.0001$; Table 2).

The minimum turning radius, R_{min}, was significantly predicted by body form ($p = 0.017$), postural reconfiguration ($p = 0.004$), and the composite model containing both body form and postural reconfiguration variables ($p < 0.0001$; Table 3 and Fig. 8). Examining body form, R_{min} increased with increasing F_b. During postural reconfiguration, R_{min} increased with β_4, β_5, δ_3, and δ_6 while it decreased with β_3. In the composite model, β_4 remained significant; in addition, m_b and β_3^* became significant.

Speed on the path of the CR, U_{cr}, was not significantly predicted by any body form variables alone; however, it was significantly predicted by both the postural reconfiguration ($p = 0.01$) and the

Table 2
Turning performance of juvenile leopard sharks, *Triakis semifasciata* ($n = 9$).

	Mean	S.E.
R_{min} (cm)	0.18	0.035
R_{min}^* (L)	0.006	0.0016
U_{cr} (cm s^{-1})	25.3	1.77
U_{cr}^* (L s^{-1})	0.78	0.086
U_r (cm s^{-1})	38.0	2.12
U_r^* (L s^{-1})	1.16	0.106
ϕ_{max} (rad)	1.75	0.121
ϕ_{max}^* (rad cm^{-1})	4.37	0.439
ω_a (rad s^{-1})	3.26	0.406
ω_b (rad s^{-1})	3.27	0.338
ω_{max} (rad s^{-1})	5.24	0.432

Variables normalized by body length are denoted with units of L, for body length.

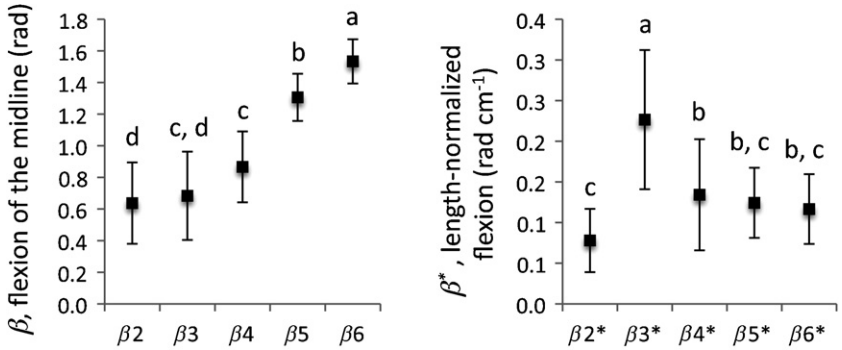

Fig. 7. Variation in postural variables along the length of the body. Flexion, β, increases significantly along the length of the body ($F_{4,40} = 29.95$; $p < 0.0001$). Length-normalized flexion, β^*, varies along the length of the body ($F_{4,40} = 7.88$; $p < 0.0001$), but the greatest flexion occurs at body point 3.

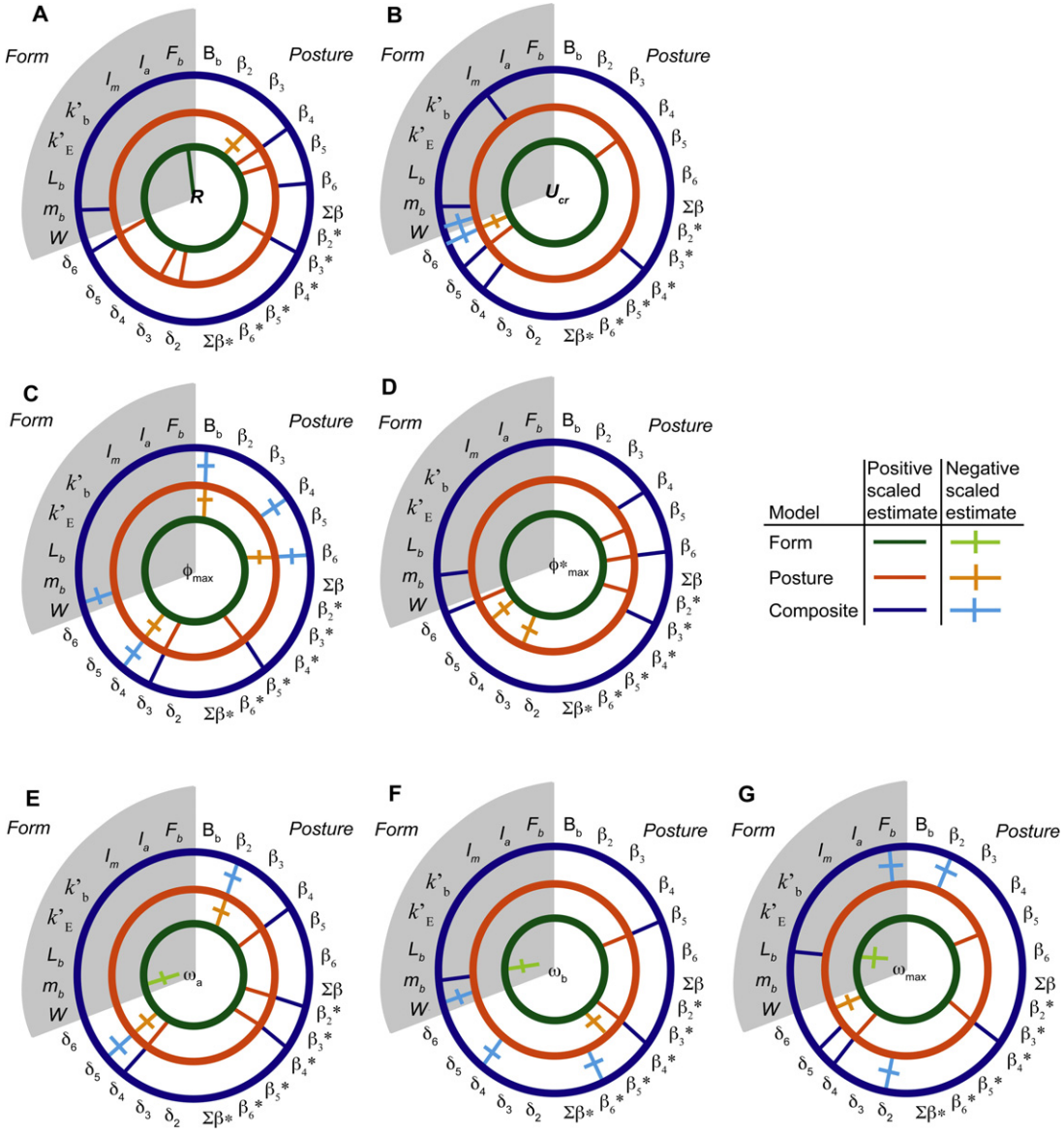

Fig. 8. Performance in turning as predicted by form and postural reconfiguration. Summary of multiple linear regression models showing how body form (variables in gray section on outer circumference) and postural reconfiguration (variables in remaining white section on outer circumference) predict the eight performance variables (variables in the center). A form or postural variable is a significant predictor ($p < 0.05$) if it is marked with a radial line. The color of the radii and the circles indicates the regression model from which the result was derived. The sign of the scaled estimate is indicated by the presence or absence of a perpendicular cross on the radial line. When only body form variables are considered (form model: green lines), they predict only the minimum turning radius, R_{min}, and the angular speeds of the head, ω_a, ω_b, and ω_{max}. When only postural variables are considered (posture model: orange lines), they predict all of the turning performance variables. When both form and postural variables are considered simultaneously (composite model: blue lines), both types predict the turning performance variables, except in one case (ω_a).

Table 3
Predicting the minimum turning radius, R_{min}, of juvenile leopard sharks, *Triakis semifasciata* ($n = 9$).

Body form			
Variables	*F* ratio	*p*	Scaled estimate
F_b	9.62	0.017	0.122
	F ratio	*p*	r^2
Whole model	9.62	0.017	0.579
Posture			
Variables	*F* ratio	*p*	Scaled estimate
β_3	1087.38	0.019	−0.013
β_4	2510.67	0.013	0.020
β_5	275.46	0.038	0.008
β_3^*	35,339.97	0.003	0.101
δ_2	15,563.42	0.005	0.081
δ_3	6781.97	0.008	0.039
δ_6	13,904.42	0.005	0.057
	F ratio	*p*	r^2
Whole model	48,767.01	0.004	1.000
Body form and posture			
Variables	*F* ratio	*p*	Scaled estimate
m_b	42.06	0.007	0.046
β_4	12.08	0.040	0.025
β_6	78.51	0.003	0.064
β_3^*	62.30	0.004	0.047
δ_6	559.96	0.000	0.106
	F ratio	*p*	r^2
Whole model	285.93	0.000	0.998

Independent variables that predict the response variable were selected from a pool of all independent variables using step-wise linear regression ($p = 0.25$ in; $p = 0.25$ out). The selected variables were then modeled in a least-squares multiple linear regression. Note that this process returns some variables with independent effects test values of $p > 0.05$; those variables should be treated cautiously.

Table 4
Predicting the path speed, U_{cr}, of the center of rotation, in juvenile leopard sharks, *Triakis semifasciata* ($n = 9$).

Body form			
Variables	*F* ratio	*p*	Scaled estimate
–		–	
	F ratio	*p*	r^2
Whole model		NS	
Posture			
Variables	*F* ratio	*p*	Scaled estimate
β_4	78.64	0.003	10.070
β_5^*	4.50	0.124	−1.921
δ_4	8.60	0.061	2.817
δ_5	70.26	0.004	5.046
δ_6	60.14	0.005	−6.202
	F ratio	*p*	r^2
Whole model	29.12	0.010	0.980
Body form and posture			
Variables	*F* ratio	*p*	Scaled estimate
m_b	9728.358	0.007	14.207
W	9004.748	0.007	−19.563
I_m	1770.814	0.015	2.780
β_4^*	203,947.5	0.001	8.742
δ_4	20,893.14	0.004	2.370
δ_5	190,625.5	0.002	6.470
δ_6	60,211.24	0.003	−9.276
	F ratio	*p*	r^2
Whole model	78,833.95	0.003	1.000

Independent variables that predict the response variable were selected from a pool of all independent variables using step-wise linear regression ($p = 0.25$ in; $p = 0.25$ out). The selected variables were then modeled in a least-squares multiple linear regression. Note that this process returns some variables with independent effects test values of $p > 0.05$; those variables should be treated cautiously.

composite model ($p = 0.003$; Table 4 and Fig. 8). In the posture model, δ_5 significantly increased with U_{cr}, but δ_6 decreased. Similarly, β_4 increased with U_{cr}. In the composite model, three body form variables changed significantly with U_{cr} (m_b, W, and I_m), and β_4^* significantly increased. Both δ_4 and δ_5 increased significantly while δ_6 decreased.

The maximal turning angle of the CR, ϕ_{max}, was significantly predicted by both the posture ($p < 0.0001$) and the composite model ($p < 0.0001$; Table 5 and Fig. 8). In the posture model, B_b and β_6 were all negatively related to ϕ_{max}, while β_5^* was positively related. Anteriorly on the body at δ_3, there was a significant positive relation with ϕ_{max}, while more posteriorly at δ_4, there was a negative relation. In the composite model body form, W increased significantly with ϕ_{max}. Postural reconfiguration variables B_b, β_4, and β_6 were all negatively related to ϕ_{max}, but β_5^* was positively related. The lag time variables showed the same statistical relation with ϕ_{max} as in the posture model.

The length-normalized maximum turning angle of the CR, ϕ_{max}^*, was significantly predicted by the posture model ($p = 0.004$) and the composite model ($p = 0.004$; Table 6 and Fig. 8). Body flexion β_5, β_6, and β_2^* increased significantly with ϕ_{max}^* in the posture model. Lag time variables δ_3 and δ_5 significantly decreased with ϕ_{max}^*. One body form variable, m_b, was positively related to ϕ_{max}^* in the composite model. Posture variables β_4, β_6, β_3^*, and δ_6 were all also positively related to ϕ_{max}^*.

Primary angular speed of the head in yaw, ω_a, was significantly predicted by body form ($p = 0.002$), postural reconfiguration ($p = 0.005$), and the composite model ($p = 0.001$; Table 7 and Fig. 8). W was significantly and negatively related to ω_a in the body form model. In the posture model, β_2 was negatively related to ω_a, but β_4 was positively related. Both β_2^* and β_4^* were positively related to ω_a. Lag δ_5 was negatively related to ω_a. There were no significant body form variables in the composite model. Body flexion β_2 was negatively related to ω_a in the composite model; β_4, β_2^*, and β_4^* were all positively related to ω_a as in the posture model.

Secondary angular speed of the head in yaw, ω_b, was significantly predicted by body form ($p = 0.0028$), posture ($p = 0.0006$), and the composite model ($p = 0.011$; Table 8 and Fig. 8). Mass of the body, m_b, was negatively related to ω_b in the body form model. Flexion variable β_5 was positively related in the posture model; however, β_5^* was negatively related while β_4^* was positively related. Two body form variables, m_b and W, were significant in the composite model. Flexion variables β_5 and β_4^* were positively related but β_6^* was negatively related to ω_b.

Body form ($p = 0.034$), posture ($p = 0.0009$), and the composite model ($p < 0.0001$) significantly predicted maximum angular speed of the head, ω_{max}, during a yaw turn (Table 9 and Fig. 8). In the body form model, L_b was negatively related to ω_{max}. Length-normalized flexion β_4^* was positively related to ω_{max}. Both δ_4 and δ_5 were positively related to ω_{max} but δ_6 was negatively related. In the composite model, two body form variables, L_b and F_b, significantly influenced ω_{max}. Flexion variable β_2 was negatively related to ω_{max}, while β_4^* was positively related. In the composite model, δ_2 was negatively related to ω_{max}, while δ_4 and δ_5 were positively related.

4. Discussion

In leopard sharks, turns are under the complex control of multiple variables that describe how the body is reconfiguring (Fig. 8).

Table 5
Predicting the maximum turning angle, ϕ_{max}, of the center of rotation in juvenile leopard sharks, *Triakis semifasciata* ($n = 9$).

Body form			
Variables	*F* ratio	*p*	Scaled estimate
–		–	
	F ratio	*p*	r^2
Whole model		NS	
Posture			
Variables	*F* ratio	*p*	Scaled estimate
B_b	1776.38	0.001	−0.503
β_6	230.48	0.004	−0.264
$\Sigma\beta$	8.19	0.104	−0.024
β_5^*	646.64	0.002	0.325
δ_3	955.99	0.001	0.230
δ_4	2632.43	0.000	−0.681
	F ratio	*p*	r^2
Whole model	1144.64	0.001	1.000
Body form and posture			
Variables	*F* ratio	*p*	Scaled estimate
W	6363.31	0.008	−0.074
B_b	1,118,036.00	0.001	−0.494
β_4	798.31	0.023	−0.011
β_6	97,340.90	0.002	−0.250
β_5^*	42,758.40	0.003	0.244
δ_3	566,437.50	0.001	0.242
δ_4	1,152,223.00	0.001	−0.700
	F ratio	*p*	r^2
Whole model	691,643.80	0.001	1.000

Independent variables that predict the response variable were selected from a pool of all independent variables using step-wise linear regression ($p = 0.25$ in; $p = 0.25$ out). The selected variables were then modeled in a least-squares multiple linear regression. Note that this process returns some variables with independent effects test values of $p > 0.05$; those variables should be treated cautiously.

Table 6
Predicting the length-normalized maximum turning angle, ϕ_{max}^*, of the center of rotation in juvenile leopard sharks, *Triakis semifasciata* ($n = 9$).

Body form			
Variables	*F* ratio	*p*	Scaled estimate
–		–	
	F ratio	*p*	r^2
Whole model		NS	
Posture			
Variables	*F* ratio	*p*	Scaled estimate
β_5	9011.20	0.007	0.500
β_6	20,546.68	0.004	0.823
β_2^*	1515.23	0.016	0.822
$\Sigma\beta^*$	24.20	0.128	−0.140
δ_3	12,812.79	0.006	−1.579
δ_5	1639.24	0.016	−0.183
δ_6	269.14	0.039	0.122
	F ratio	*p*	r^2
Whole model	47,478.76	0.004	1.000
Body form and posture			
Variables	*F* ratio	*p*	Scaled estimate
m_b	42.06	0.007	0.046
β_4	12.08	0.040	0.025
β_6	78.51	0.003	0.064
β_3^*	62.30	0.004	0.047
δ_6	559.96	0.000	0.106
	F ratio	*p*	r^2
Whole model	285.93	0.004	1.000

Independent variables that predict the response variable were selected from a pool of all independent variables using step-wise linear regression ($p = 0.25$ in; $p = 0.25$ out). The selected variables were then modeled in a least-squares multiple linear regression. Note that this process returns some variables with independent effects test values of $p > 0.05$; those variables should be treated cautiously.

Dynamic reconfiguration of posture, as measured by flexion of the midline, β, and the lag time of the flexion, δ (Fig. 6), was a consistent and strong predictor of turning performance. Body form was predictive to a lesser degree. Since we had shown previously that body form across five species of shark predicted more than half of the variance in the body-bending coefficient, B_b, during turns (Porter et al., 2009), we expected it to explain more of the variation in turning performance. Instead, we see that postural reconfiguration is the most important determinant of yaw turning performance in leopard sharks.

We have made progress in understanding the basis of locomotor maneuvers by quantifying the turning performance of leopard sharks in a variety of ways (Figs. 2–5). A surprising result is the high performance, compared to other aquatic vertebrates, measured by the minimum turning radius, R_{min}, which is small in absolute terms (mean of 0.18 cm) and miniscule when normalized by L_b (mean of 0.006 L_b, reported as R_{min}^* in Table 2). The small values of R_{min} and R_{min}^* rival those measured in swimming whirly-gig beetles (Fish, 1999) and small fish with $L_b < 10$ cm (for review, see Domenici, 2001). Thus leopard sharks, with L_b ranging from 25 to 49 cm in this study, are among the best aquatic turners in terms of R_{min}.

The reason for these small values of R_{min} in leopard sharks may, in part, stem from the fact that the leopard sharks were swimming within a confined aquarium. They had room to swim before turning, and turning always took place in response to avoiding a wall. While it might be argued that these conditions are artificial, there can be little doubt that leopard sharks have the capacity to be highly maneuverable.

Leopard sharks also showed an unexpected scaling of R_{min} with L_b. For fish and cetaceans, R_{min} increases linearly with increases in L_b when compared interspecifically (Domenici, 2001). This was not the case for the intraspecific changes in R_{min} measured in leopard sharks, where L_b was not predictive of this measure of swimming performance. On the other hand, a different measure of turning performance, the maximum angular speed of the head in yaw, ω_{max}, did scale with L_b within leopard sharks as predicted by interspecific scaling in fishes (Domenici, 2001). The form model returned L_b as the only significant predictor of ω_{max} (Table 9). In leopard sharks, as in fishes, ω_{max} decreases as L_b increases when compared intraspecifically. Since the magnitude of ω_{max} in leopard sharks is comparable to that of similarly sized fishes, leopard sharks perform, as measured by ω_{max}, as predicted (Domenici, 2001).

The volitional turns in leopard sharks examined here produced angular turning speeds (3.26 rad s^{-1} for mean ω_a and 5.24 rad s^{-1} for mean ω_{max}) that were comparable to those measured in slow escape turns previously reported for sharks. Slow and fast escape-type turns were described in the spiny dogfish, *Squalus acanthias* (Domenici et al., 2004). The slow turns resulted in ω_a and ω_{max} of 4.68 and 8.42 rad s^{-1}, respectively. The fast turns resulted in ω_a and ω_{max} of 7.94 and 14.99 rad s^{-1}, respectively, producing escapes that were nearly twice as fast as the slow responses. The fast escape responses of *S. acanthias*, elicited by startling the shark with a pole, were faster than those reported in other carcharhiniform species whose startle responses were elicited by electric stimuli. The ω_{max} reported for *Sphryna lewini* and *Carcharhinus plumbeus* were 8.2 rad s^{-1} and 4.3 rad s^{-1}, respectively (Kajiura et al., 2003). Despite the wide range of total lengths of individuals in these

Table 7
Predicting the initial angular speed of the head, ω_a, in yaw in turning juvenile leopard sharks, *Triakis semifasciata* ($n = 9$).

Body form			
Variables	*F* ratio	*p*	Scaled estimate
W	24.92	0.0016	−0.978
	F ratio	*p*	r^2
Whole model	24.92	0.002	0.781

Posture			
Variables	*F* ratio	*p*	Scaled estimate
β_2	4253.43	0.010	−0.864
β_3	7.08	0.229	−0.023
β_4	206.60	0.044	0.312
β_2^*	1729.79	0.015	0.744
β_4^*	728.96	0.024	0.787
δ_4	72.41	0.075	0.068
δ_5	882.02	0.021	−0.179
	F ratio	*p*	r^2
Whole model	21,330.05	0.005	1.000

Body form and posture			
Variables	*F* ratio	*p*	Scaled estimate
k_b'	118.54	0.058	−0.028
β_2	56,737.26	0.003	−0.858
β_4	5966.49	0.008	0.348
β_2^*	25,048.50	0.004	0.731
β_4^*	10,385.90	0.006	0.736
δ_4	1158.99	0.019	0.071
δ_5	12,693.86	0.006	−0.175
	F ratio	*p*	r^2
Whole model	315,463.20	0.001	1.000

Independent variables that predict the response variable were selected from a pool of all independent variables using step-wise linear regression ($p = 0.25$ in; $p = 0.25$ out). The selected variables were then modeled in a least-squares multiple linear regression. Note that this process returns some variables with independent effects test values of $p > 0.05$; those variables should be treated cautiously.

Table 8
Predicting the secondary angular speed of the head, ω_b, in yaw in turning juvenile leopard sharks, *Triakis semifasciata* ($n = 9$).

Body Form			
Variables	*F* ratio	*p*	Scaled estimate
m_b	7.67	0.028	−4.761
	F ratio	*p*	r^2
Whole model	7.67	0.028	0.523

Posture			
Variables	*F* ratio	*p*	Scaled estimate
β_5	60.57	0.003	1.473
β_4^*	79.16	0.004	3.447
β_5^*	4.55	0.019	−0.820
β_6^*	6.41	0.085	−0.930
δ_4	21.48	0.123	−0.641
	F ratio	*p*	r^2
Whole model	42.41	0.006	0.986

Body form and posture			
Variables	*F* ratio	*p*	Scaled estimate
m_b	252.41	0.040	3.722
W	184.38	0.047	−4.187
β_5	1198.64	0.018	2.323
$\Sigma\beta$	85.93	0.068	0.466
β_4^*	4782.08	0.009	4.156
β_6^*	454.75	0.030	−2.971
δ_4	2272.82	0.013	−0.749
	F ratio	*p*	r^2
Whole model	5156.64	0.011	1.000

Independent variables that predict the response variable were selected from a pool of all independent variables using step-wise linear regression ($p = 0.25$ in; $p = 0.25$ out). The selected variables were then modeled in a least-squares multiple linear regression. Note that this process returns some variables with independent effects test values of $p > 0.05$; those variables should be treated cautiously.

species (34.8 cm mean L_b of *T. semifasciata* in this study to 75.1 cm mean L_b of *S. lewini* in Kajiura et al., 2003), these species share similar slow turning speeds but differ in their behavioral ecology, from the coastal migrations and benthic interactions of leopard sharks to the pelagic zone cruising of hammerheads.

When we examine performance measures together, we get a more complete picture of how leopard sharks turn. They can swim in a straight line and then quickly turn "on a dime", rotating with a R_{min} that approaches zero, do so with a large turning angle, ϕ_{max}, a rapid ω_{max}, and, before or after the braking required for such a maneuver, a high translational speed of the body's center of rotation, U_{cr}. Sharks vary their turning behavior (Table 2), with body flexion variables, β and β^*, both positively and negatively correlated with the performance variables (Fig. 8).

In terms of the control of turning behavior, the differences in positive and negative correlations of performance variables with both form and postural variables mean that trade-offs in turning performance abound (Fig. 9). For example, if a shark wanted to decrease R_{min}, it might increase its maximal body flexion at points 4 and 6, β_4 and β_6, respectively (Fig. 8). However, in so doing, ϕ would decrease (Fig. 8). Choosing instead to maximize its ω_{max}, the shark might increase the lag time at points 4 and 5, δ_4 and δ_5, respectively (Fig. 8). Those changes would also increase the U_{cr} but, at the same time, they would lower ϕ_{max} (Fig. 8).

Which aspects of turning performance matter most to leopard sharks depends on their ecological situation. Leopard sharks, which occur inshore throughout the eastern Pacific of the northern hemisphere, are constantly on the move, swimming with the tides into the muddy littoral zone to forage for benthic invertebrates and coastal fishes (Ackerman et al., 2000). While foraging in narrow coastal channels and shallow mud flats, leopard sharks likely rely on their ability to tightly maneuver within confined distances. Since, under these circumstances, elusive prey can be trapped in narrow spaces, it is likely that leopard sharks take advantage of small values of R_{min} and large values of ϕ at the expense of the speed-related variable ω_{max}. In deeper water situations, during daily tidal movements or seasonal coastal movements, rotational and translational speed are likely to be of primary concern, since neither prey nor predators are limited by substrate interactions (Domenici, 2001).

Individual leopard sharks in the Elkhorn Slough estuary of California differed in their use of habitat, with some preferring tidal channels and others preferring mud flats; periods of active foraging within a small area were often punctuated by rapid and directed movements to a different habitat within the slough, often against the tides (Carlisle and Starr, 2009). A range of depths were chosen by the sharks while they remained in the slough from spring to fall; many departed for more oceanic bays during the winter while some adults and juveniles remained in the slough throughout the year (Carlisle and Starr, 2009). Littoral habitats with channels, tides, and low water depths require high degrees of maneuverability to navigate. Couple those hydrological challenges with the requirements of foraging for active invertebrate and vertebrate prey and it seems reasonable to predict that yaw turning – and the ability to adjust turning performance based on ecological circumstance – is a key behavior in the ecology of leopard sharks.

Table 9
Predicting the maximum angular speed of the head, ω_{max}, in yaw in turning juvenile leopard sharks, *Triakis semifasciata* ($n = 9$).

Body form			
Variables	*F* ratio	*p*	Scaled estimate
L_b	6.94	0.034	−1.098
	F ratio	*p*	r^2
Whole model	6.94	0.034	0.498

Posture			
Variables	*F* ratio	*p*	Scaled estimate
β_2^*	3.11	0.220	0.280
β_4^*	119.04	0.008	2.293
β_5^*	8.39	0.101	−0.418
δ_4	26.01	0.036	0.620
δ_5	45.01	0.022	0.675
δ_6	50.69	0.019	−0.747
	F ratio	*p*	r^2
Whole model	108.29	0.009	0.997

Body form and posture			
Variables	*F* ratio	*p*	Scaled estimate
L_b	121,915.40	0.002	0.392
F_b	350,679.70	0.001	−0.705
β_2	50,827.64	0.003	−0.231
β_4^*	3,092,143.00	0.000	2.496
δ_2	2369.48	0.013	−0.034
δ_4	171,339.30	0.002	0.420
δ_5	578,050.00	0.001	0.502
	F ratio	*p*	r^2
Whole model	1,275,544.00	0.001	1.000

Independent variables that predict the response variable were selected from a pool of all independent variables using step-wise linear regression ($p = 0.25$ in; $p = 0.25$ out). The selected variables were then modeled in a least-squares multiple linear regression. Note that this process returns some variables with independent effects test values of $p > 0.05$; those variables should be treated cautiously.

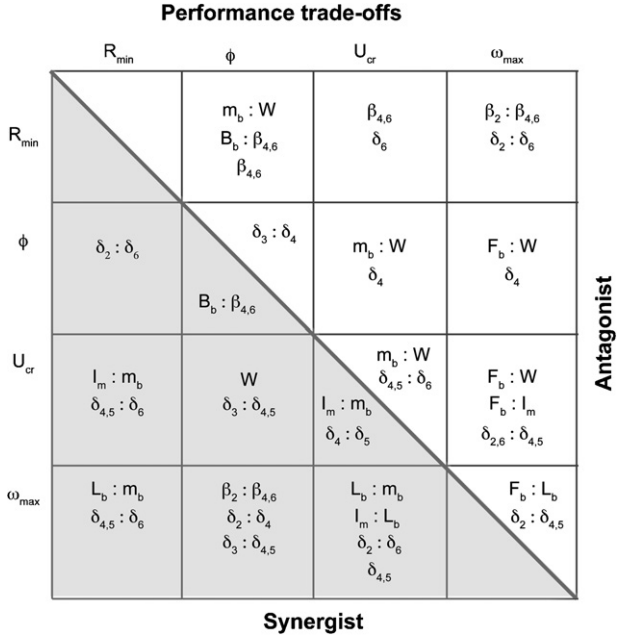

Fig. 9. Trade-offs and synergisms among the variables that characterize turning performance. Trade-offs (antagonisms) are shown in the upper diagonals (white background). Synergisms are shown in the lower diagonals (gray background). If form or posture variables appear in a pair, separated by a colon, it means that those two variables are causally related. If a form or posture variable is present in an antagonist cell, it means that changes in that variable will simultaneously impose opposite pressures on turning performance by affecting multiple variables by which we have measured turning performance. If a form or posture variable is present in a synergist cell, it means that changes in that variable will simultaneously enhance multiple variables of turning performance.

One interpretation of the observation that the angular speed of slow turns is similar across species and ecologies is that that behavior is evolutionarily conserved. Conservation is a hypothesis that states that a trait arose in a shared ancestor and was neither lost nor changed in descendent lineages. Conservation can occur when selection pressures on the trait in question are constant across time and among species; conservation may also occur if the trait has low heritability or is genetically linked to other traits experiencing strong stabilizing selection. Which of these scenarios is more likely is impossible to say without careful investigations of the selection on and genetics of natural populations of sharks.

Postural reconfiguration, as measured by B_b alone, has been shown to predict turning velocity in other species of sharks. Greater values of B_b were correlated with higher angular head speeds in *S. lewini* and *C. plumbeus* ($\omega = 8.2$ rad s^{-1} and 4.3 rad s^{-1}, respectively) even though the turning radius was not significantly different between those species (Kajiura et al., 2003). We noted in this present study that when other postural variables were measured, such as flexion, B_b was predictive of only one performance variable, ϕ_{max} (Fig. 7). This suggests, at least for leopard sharks, that B_b, a variable that accounts for the shape of the whole body, results from the more mechanically proximal local body flexion.

Reconfiguration, or change in shape, occurs within an individual as it self-propels, maneuvers, and develops; reconfiguration also occurs among populations as they evolve. Reconfiguration can be mathematically partitioned into three types: (i) undulation, (ii) posture, and (iii) form (Long et al., 2010). While form reconfiguration, the change in the static shape of the body, occurs over developmental and evolutionary time, individual differences within a population allow assessment of form reconfiguration at a given time. Undulatory and postural reconfigurations, changes in the dynamic shape of the body, interact to produce steady locomotion and maneuvers within or between behaviors. Analysis of the volitional turning of leopard sharks showed the greater importance of postural reconfiguration compared to undulatory reconfiguration in generating this routine maneuver (Long et al., 2010). Intriguingly, in that same study postural reconfiguration, as measured by the maximal body-bending coefficient, B_b, was uncorrelated with the stiffness index of cantilevered bending, k_b', a mechanically motivated measure of form.

In summary, leopard sharks control their turning performance by modulating the group of postural variables that include body flexion and the relative timing of that flexion. Turning performance is also affected by form variables that cannot be modulated: body mass, body width, body length, and fineness ratio. The general picture that emerges is that the body reconfigures over different time scales and reconfiguration drives turning performance. With this information, we may now begin to construct mechanical models of turning in sharks. A model could include a mechanism for the shark to flex its body, control the magnitude and timing of that flexion regionally, and have the reconfiguring body create inertial force, internal muscular and elastic force, and external fluid force coupled with the internal forces. By altering the parameters for body form, this model would allow us to test the relative importance of form and posture, as well as differences in performance among different species of shark.

Acknowledgments

We thank the institution and people who made work on live sharks possible: Santa Monica Pier Aquarium, Santa Monica, CA

(Jose Bacallao and staff). Data collection went more smoothly with the helping hands of Jessica Alvarez, Nick Tan, Sabreena Kasbati, Andrew Clark, and Ruth Porter. A special thanks to the UCI Biomechanics Group, especially the Summers and McHenry Labs for their support and guidance. Funding for this research was provided by grants from the American Elasmobranch Society and the Society of Integrative and Comparative Biology to M.E.P., and the National Science Foundation to Adam P. Summers (IBM-0317155), J.H.L. (DBI-0442269), and M.E.P. and J.H.L. (IOS-922605).

Appendix A. Supplementary data

Supplementary data associated with this article can be found in the online version at doi:10.1016/j.zool.2011.06.001.

References

Ackerman, J.T., Kondratieff, M.C., Matern, S.A., Cech, J.J., 2000. Tidal influence of statial dynamics of leopard sharks, *Triakis semifasciata*, in Tomales Bay, California. Environ. Biol. Fishes 58, 33–43.

Azizi, E., Landberg, T., 2002. Effects of metamorphosis on the aquatic escape response of the two-lined salamander (*Eurycea bislineata*). J. Exp. Biol. 205, 841–849.

Carlisle, A.B., Starr, R.M., 2009. Habitat use, residency, and seasonal distribution of female leopard sharks *Triakis semifasciata* in Elkhorn Slough, California. Mar. Ecol. Prog. Ser. 380, 213–228.

Domenici, P., 2001. The scaling of locomotor performance in predator–prey encounters: from fish to killer whales. Comp. Physiol. Biochem. A 13, 169–182.

Domenici, P., Standen, E.M., Levine, R.P., 2004. Escape manoeuvers in the spiny dogfish (*Squalus acanthias*). J. Exp. Biol. 207, 2339–2349.

Fish, F.E., 1999. Performance constraints on the maneuverability of flexible and rigid biological systems. In: Proceedings of the 11th International Symposium on Unmanned Untethered Submersible Technology, Autonomous Undersea Systems Institute, Durham, NH, pp. 394–406.

Fish, F.E., Hurley, J., Costa, D.P., 2003. Maneuverability by the sea lion *Zalophus californianus*: turning performance of an unstable body design. J. Exp. Biol. 206, 667–674.

Gautrais, J., Jost, C., Soria, M., Campo, A., Motsch, S., Fournier, R., Blanco, S., Theraulaz, G., 2009. Analyzing fish movement as a persistent turning walker. J. Math. Biol. 58, 429–445.

Kajiura, S.M., Forni, J.B., Summers, A., 2003. Maneuvering in juvenile carcharhinid and sphyrnid sharks: the role of the hammerhead shark cephalofoil. Zoology 106, 19–28.

Long Jr., J.H., 1995. Morphology, mechanics, and locomotion: the relation between the notochord and swimming motions in sturgeon. Environ. Biol. Fishes 44, 199–211.

Long Jr., J.H., 1998. Muscles, elastic energy, and the dynamics of body stiffness in swimming eels. Am. Zool. 38, 771–792.

Long Jr., J.H., Adcock, B., Root, R.G., 2002a. Force transmission via axial tendons in undulating fish: a dynamic analysis. Comp. Biochem. Physiol. A 133, 911–929.

Long Jr., J.H., Koob-Emunds, M., Sinwell, B., Koob, T.J., 2002b. The notochord of hagfish *Myxine glutinosa*: visco-elastic properties and mechanical functions during steady swimming. J. Exp. Biol. 205, 3819–3831.

Long Jr., J.H., Lammert, A.C., Pell, C.A., Kemp, M., Strother, J.A., Crenshaw, H.C., McHenry, M.J., 2004. A navigational primitive: biorobotic implementation of cycloptic helical klinotaxis in planar motion. IEEE J. Oceanic Eng. 29, 795–806.

Long Jr., J.H., Porter, M.E., Root, R.G., Liew, C.W., 2010. Go reconfigure: how fish change shape as they swim and evolve. Integr. Comp. Biol. 50, 1120–1139.

Nguyen, Q.S., Heo, S., Park, H.C., Goo, N.S., Byun, D., 2009. Cruise and turning performance of an improved fish robot actuated by piezoceramic actuators. Proc. SPIE 7288, 72880J.

Porter, M.E., Roque, C.M., Long Jr., J.H., 2009. Turning maneuvers in sharks: predicting body curvature from axial morphology. J. Morph. 270, 954–965.

Root, R.G., Courtland, H.-W., Shepherd, W., Long Jr., J.H., 2007. Flapping flexible fish: periodic and secular body reconfigurations in swimming lamprey, *Petromyzon marinus*. Exp. Fluids 43, 779–797.

Smith, S.E., 1984. Timing of vertebral-band deposition in tetracycline-injected leopard sharks. Trans. Am. Fish Soc. 113, 308–313.

Tytell, E.D., Lauder, G.V., 2008. Hydrodynamics of the escape response in bluegill sunfish, *Lepomis macrochirus*. J. Exp. Biol. 211, 3359–3369.

Walker, J.A., 2000. Does a rigid body limit maneuverability? J. Exp. Biol. 22, 3391–3396.

Webb, P.W., 1984. Body form, locomotion, and foraging in aquatic vertebrates. Am. Zool. 24, 107–120.

Webb, P.W., 2004. Maneuverability—general issues. IEEE J. Oceanic Eng. 29, 547–555.

Webb, P.W., Fairchild, A.G., 2001. Performance and maneuverability of three species of teleostean fishes. Can. J. Zool. 79, 1866–1877.

Wu, C., Wang, L., 2010. Where is the rudder of a fish? The mechanism of swimming and control of self-propelled fish school. Acta Mech. Sin. 26, 45–65.

Wu, G., Yang, Y., Zeng, L., 2008. Routine turning maneuvers of koi carp *Cyprinus carpio* koi: effects of turning rate on kinematics and hydrodynamics. J. Exp. Biol. 210, 4379–4389.